Microstructure Characterization of thermal barrier coating deposits – practical models from measurements

J. Ilavsky, Argonne/USA, A. J. Allen, Gaithersburg/USA, T. Dobbins, Louisiana/USA, A. Kulkarni and H. Herman, Stony Brook/USA

Advances in the functional properties of thermal barrier coating (TBC) deposits are important for increasing the efficiency of, and reducing emissions from both stationary and aircraft turbine engines. Computer modeling is the preferred method for developing new materials with minimum cost and development time. However, modeling of TBCs is complex and must take into account interactions among the layers and with the substrate, in-service phase changes, oxidation, and stress development. Understanding the microstructure of the ceramic layer is important for building these models, as it strongly influences the properties responsible for the basic TBC function – thermal resistance. As is well known the ceramic microstructure changes in service, potentially leading to coating and engine failure. A major challenge is ensuring that the model reliably describes the actual material. Thus, it is important to develop representative models, which can be related to real practical coating systems.
We present such a model. It has been developed to interpret small-angle X-ray scattering data that characterize TBC ceramic deposit microstructures. This model is also suitable for incorporation into computer algorithms such as are used in finite-element analysis. Quantitative parameters that describe the microstructure changes occurring under service conditions are readily obtainable for current systems, and these can then be re-measured for future materials of interest.

1 Introduction

Advances in computer finite element models (FEM) have been rapid in the last few years, facilitated by the availability of ever increasing processing speed and random access memory. Different philosophies have developed on how to calculate the materials properties from model representations of the microstructure.[1-4] Many models currently used in materials design are modifications of standard models developed for engineering applications, and most are quite simple in their underlying assumptions.

However, materials microstructure problems on the microscopic scale are significantly different and more complex in geometrical organization than are engineering structure problems on the macroscopic scale, such as the modeling of bridges and other engineering components. For example, the microstructures faced in materials design frequently do not conform well to a simple geometrical grid. Therefore, it was recognized early on that simplified microstructure models are necessary. However, when such an approach is taken, a major question arises as to how well the simplified model actually describes the natural phenomena involved. Another issue is whether meaningful, realistic and quantitative measurements of real materials resulting in applicable model parameters are available, so the engineering properties calculated from the model represent the real materials properties.

Here we present a simplified microstructure model of complex ceramic coatings developed for the analysis of small-angle scattering measurements, mainly for data obtained on an ultra small angle X-ray scattering (USAXS) instrument. This model, however, may be suitable for use in FEM methods, and, since the measured microstructure parameters are now available, it may be highly relevant for practice.

2 Theory

2.1 Microstructure

Multiple populations of voids can be identified in thermally sprayed ceramics and metallic deposits. While categorization and names somehow vary, one of the most common is division by process of formation into. 5-11

1. Interlamellar voids - created during deposition between the lamellae in areas of poor contact. These can be approximated as “disks”- or “oblate ellipsoids,” with the large dimension on the order of 1/10 of the splat diameter and the small dimension on the order of 1/10 of splat thickness. These voids follow the surface of the splats, limiting the validity of disk or oblate ellipsoid approximation. They are predominantly parallel having their long dimension along the substrate plane.
2. Intralamellar voids – usually associated with stress relaxation of the splats on cooling, often called cracks. These voids propagate predominantly vertically through the splats and, while most are small and contained within one splat, the large ones can propagate through the whole splat thickness. Sometimes they can be observed on the top surfaces of single splats as network of hairline cracks.[12] The model approximates them as oblate ellipsoids. Careful observations of high-resolution scanning electron microscope (SEM) images indicate that their aspect ratio is at least 1/10.
3. Globular pores – relatively large voids of close-to-spherical shape are often observed in the images of cross sections. Even though many may be the result of sample preparation - breakage of parts of splats combined with pull out of weakly bonded of unmelted particles, previous studies, using methods that do not

require polishing (such as small-angle neutron scattering or X-ray tomography), proved that these are present in the undisturbed microstructure.[13] These voids have been observed in a wide range of sizes - up to feedstock powder size and down to the resolution limit of the imaging technique. For the purpose of this model, we assume these are generally larger than splat thickness.

2.2 Model

The following criteria were observed for the model and computer code design:

- Be reasonably realistic, including the fact that, while the anisotropic voids exhibit preferred orientation, they are not exactly aligned – therefore distribution of orientations is necessary.
- Use idealizations of particle shapes, for which small-angle scattering can be reasonably well calculated.
- Allow use of numerical methods to "optimize" the model parameters. Least square fitting was selected for simplicity.
- Formulate algorithms that can be run in a realistic time-frame using currently available computer systems, given that the scattered intensity calculation for anisotropic, non-randomly oriented particles requires multiple embedded numerical integrals.

These requirements have resulted in the following model characteristics:

- Four independent (and mathematically equivalent) populations of voids.
- Each population composed of spheroidal particles with axes R_0, R_0, βR_0. For this shape there are analytical formulae to calculate the small-angle scattering that are valid for a sufficiently large range of aspect ratios, at least from $\beta = 1/25$ to $\beta = 25$.
- Particle size distributions are available – the code has options for a Gaussian size distribution with a user defined number of bins and width, or a simplified triangular size distribution.
- The coordinate system was selected with the x axis in the spray direction (perpendicular to the substrate plane) and with the y and z axes lying in the substrate plane (Fig. 1).
- The orientation of a single particle in space is described by that of the βR_0 axis with respect to the coordinate system by two independent angles α and ω, α being the angle between the βR_0 direction and the x axis, ω being the angle within the substrate plane, between the y axis and the βR_0 direction (Fig. 1). As an approximation we assume that the two angles, α and ω, are independent, and the probability of finding a particle in any particular orientation can be described satisfactorily by multiplying the probabilities for the two angles: $P(\alpha,\omega) = P(\alpha) * P(\omega)$.

Figure 2 shows the SEM microstructure to be characterized by the presented model. In Fig. 3 the highlighted ellipses represent examples of cross sections for the model voids, all with aspect ratio 1/10 or 1 (used in this case).

The code for calculating the small-angle scattering from the model in an arbitrary direction with respect to the axes system was designed in Igor Pro (Wavemetrics Inc., www.wavemetrics.com)*. This package provides a suitable platform for both calculations and graphing, as the data need to be graphically compared. While the interpretive language of the package is slower than code written in C, the difference is actually not that significant (estimated to be less than a factor of 2). The advantage of using the package is the availability of a highly optimized library of mathematical functions and fitting routines. This significantly simplifies the code writing and optimization.

The code was successfully used for evaluation of data obtained on samples manufactured by electron-beam physical vapor deposition (EBPVD), thermal spray, polymers with anisotropic structure etc.

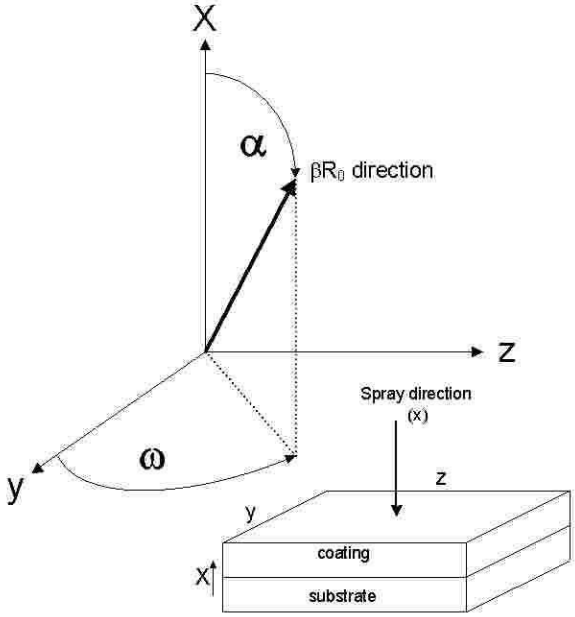

Figure 1. Axes definition and sample orientation for the model described.

2.3 Model parameters

Each population used in the model is described fully by its R_0 value, aspect ratio of particle model β, (fractional) volume of particles, and functions $P(\alpha)$ and $P(\omega)$. In the present case, we assumed that $P(\omega)$ is constant – which means that the sample is circularly-symmetric when viewed from the spray (x) direction, conditions routinely satisfied with the spray direction

* Information on commercial products is given for completeness and does not necessarily constitute or imply their endorsement by the National Institute of Standards and Technology.

perpendicular to the subtrate surface.[14] Note that both $P(\alpha)$ and $P(\omega)$ have to normalize to 1 when integrated over α from 0 to 180 degrees and ω from 0 to 360 degrees, respectively.

To provide a way to optimize $P(\alpha)$ and $P(\omega)$, we have implemented arbitrary functional formulae for these probabilities, which have proven themselves to be suitable. These functions were selected with the following requirements: a limited number of parameters (3), simple mathematical formulae, and the capacity to have an isotropic component, as well as a component peaked in any particular direction with an option to change the width of the peak. The following formulae were selected:

$P(\alpha) = C1 * (A1 * \cos(\alpha - A2) + A3)$

$P(\omega) = C2 * (B1 * \cos((\omega - B2)/2) + B3)$

A1, A2, A3 are parameters for $P(\alpha)$ and B1, B2, and B3 for $P(\omega)$. For any given A1, A3, B1 and B3, these functions are renormalized using C1 and C2.

Information on the width of the size distribution must also be included.

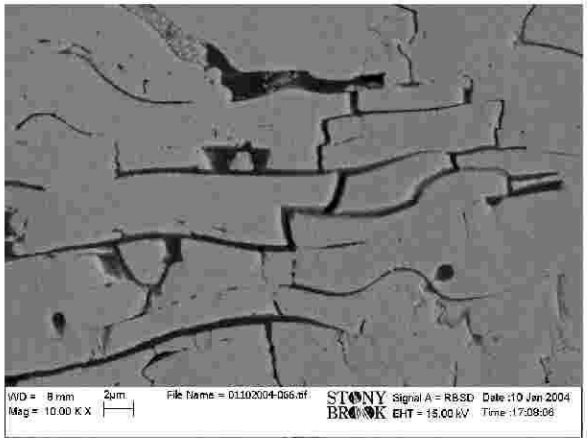

Figure 2. SEM microstructure of studied sample.

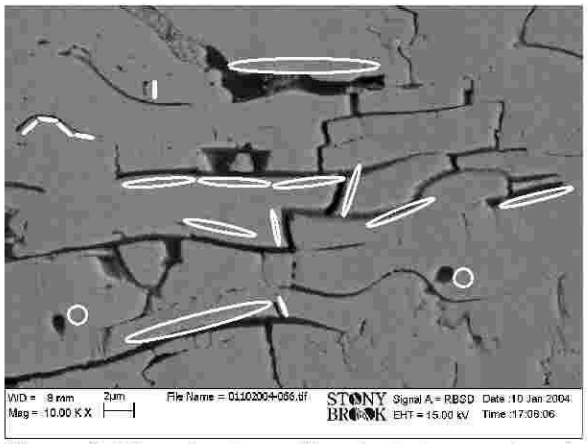

Figure 3. Microstructure with selected examples of model shapes next to voids. The ellipses represent cross section profiles of the model spherical voids or oblate ellipsoidal voids with aspect ratio 1/10.

3 Measurements

3.1 Small-angle scattering

The 2D collimated USAXS camera, built by NIST at the UNICAT sector of the Advanced Photon Source, Argonne National Laboratory, Illinois, USA, is capable of measuring scatterer sizes from about 10 nm to about 2 micrometers and simultaneously characterizing the anisotropy of the scatterer system.[15] This allows the characterization of microstructures that exhibit a wide range of void sizes.

The USAXS measurement of the anisotropic samples is a combination of two steps:

1. The scattered intensity at a fixed magnitude, q, of the scattering vector, **q**, is measured as the sample is rotated around one of the sample axis – either the x, y or z axes, as defined in Fig. 1. With the sample prepared in cross section (i.e., with the X-ray beam parallel to the substrate plane), the sample is rotated around the y axis. This records a measure of the anisotropy dominated by scatterers of a size related to the magnitude of the scattering vector **q** (see Fig. 4). We call these types of measurements azimuthal scans, and a number of these may be needed to characterize the anisotropy of complex microstructures.

2. Next the scattered intensity is measured as a function of the scattering vector **q** at selected azimuthal angles (Fig. 5). This results in small-angle scattering data sets as they are commonly understood. A number of directions may have to be selected, based on azimuthal scans, to characterize the extreme directions for various size ranges. Note that the microstructure is always characterized parallel to the direction of **q**, and that **q** bisects the angle between the incident and scatteried beams. Hence it lies approximately within the plane of the sample.

3.2 Sample

The results presented in this manuscript were obtained from a sample of thermally sprayed yttria (8% by mass)-stabilized zirconia, manufactured from Metco 204BNS* feedstock. For SEM microstructure see Fig. 2. The selected sample was part of a larger study, in which different size cuts of the same material were studied in the as-sprayed and annealed states. This particular sample was manufactured from coarse powder cut and annealed at 1200 °C for 225 h after spraying. The results presented here are intended to illustrate the capabilities of the model. It is not intended to present a detailed microstructure study here, nor to compare different methods – this will be done elsewhere.

Results, obtained during previous studies (to be published) using precision densitometry, intrusion porosimetry, image analysis and multiple small angle neutron scattering (MSANS)[16] indicate, that the total porosity of this sample is about 14%, with about 6.6% of porosity in the interlamelllar pore system, 5.9% in the globular voids and 1.5% in the intralamellar voids.

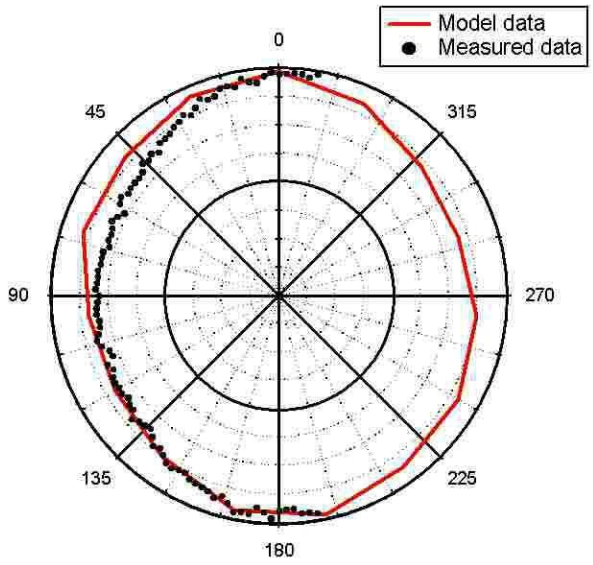

Figure 4. Observed and modeled anisotropy of the small angle scattering at q = 0.0142 A^{-1}. Data were obtained from -10° to 190° in azimuthal angle.

4 Results and discussion

4.1 Model results

Figures 4 and 5 show examples of the measured data and mode fits. Figure 5 shows the measured Intensity vs. **q** dependencies for three selected directions of **q** with respect to the x axis at 0° (where q is perpendicular to the substrate). At 90° **q** is parallel with the substrate plane, and at 45° **q** is 45° off the substrate plane. Note good agreement between the measured and modeled intensities was observed.

Figure 4 shows observed (black points) and modeled (line) anisotropy as a function of the angle α at q = 0.0142 A^{-1}. Again, generally good agreement between the observed and modeled anisotropy was observed. The scattering anisotropy was measured at several different values of q, associated with microstructural anisotropy in various void size ranges within the material. In all cases a similarly acceptable agreement was observed.

The presented results show that, within the reasonable expectations for such a simplified model, the model does predict the scattering that agrees with the measured data from the complex microstructure.

Numerical results are presented in Table 1. Note that the size distribution of the interlamellar pores – the most populous type of pores in this system – is so broad that it had to be modeled by two separate void populations with the same aspect ratio but with different radii and size distribution FWHM values.

4.2 Comparison of model results

The model predicts a total porosity of 9.9%, compared to the measured value of about 14%. This can be related to the fact that voids of sizes larger than 1 micrometer are not really visible by this technique. It is also supported by the fact that the globular voids, which (according to MSANS results) represent about 5.9% porosity, are reported by this method as being about 1%. Actually, the difference between results can very well be explained by the difference in globular pores only, since the sum of the interlamellar pores and intralamellar pores for the MSANS method

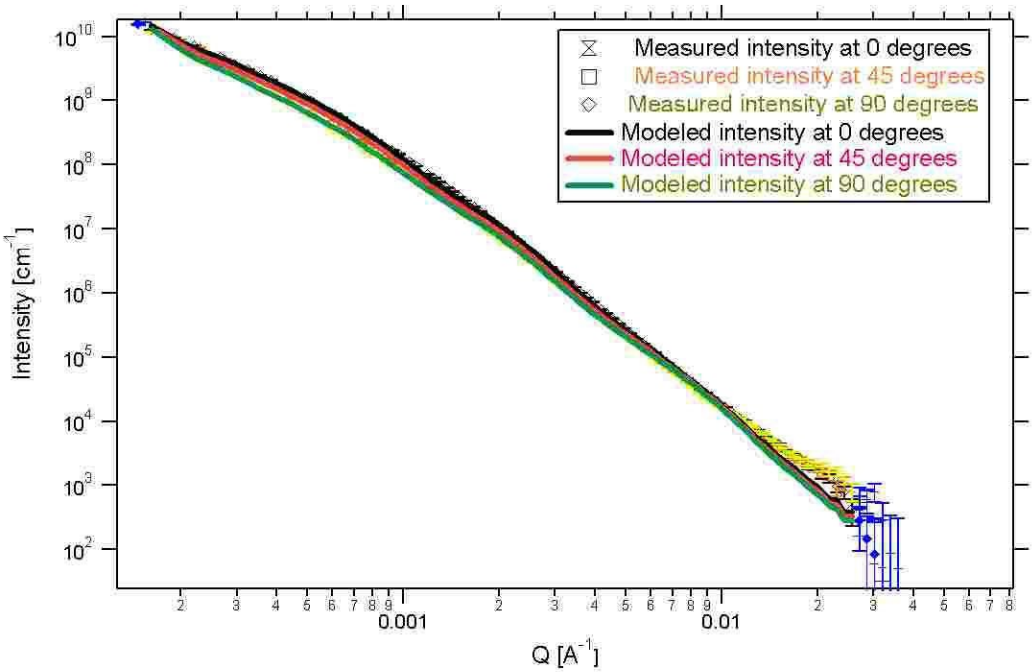

Figure 5. USAXS measured and modeled data.

Table 1. Numerical results of the model.
Note that, due to the broad distribution of sizes in the interlamellar pore system, two populations were needed to cover the range. The FWHM represent full width at half maximum for an assumed Gaussien distribution of sizes and is fixed. Estimated errors are presented in brackets.

	Volume [%]	Aspect ratio (fixed)	Radius [mm]	FWHM (fixed) [μm]	A1	A2	A3
Interlamellar pores population 1	3.9(2)	0.2	1.54(20)	0.4	0	2.14(10)	**0.66(5)**
Interlamellar pores population 2	4.5(2)	0.2	0.51(10)	0.2	0	5.82(10)	**1.27(10)**
Intralamellar pores /. cracks	0.5(2)	0.1	0.28(5)	0.1	90	2.43(10)	**1.65(10)**
Globular pores	**1.0(2)**	**1**	**2.0 (fixed)**	**0.4**	**na**	**na**	**na**

is 8.1% and for the USAXS method is 8.9%.
The two methods present similar pictures of the fractions of interlamellar/intralamellar voids in the material; in each case, the interlamellar voids dominate, with intralamellar voids (cracks) representing a significantly smaller volume fraction. Numerical differences are likely due to the different methods of anisotropy modeling and the other assumptions involved.

4.3 Use of results

The presented model can be used to generate input microstructures for FEM models. Unlike the situation for microscopic image analysis, these numerical microstructures do not need thresholding and they do not have a resolution limit for small voids. Furthermore, the model is intrinsically three dimensional and can be generated easily for any needed size domain.

5 Conclusions

The presented model provides a means of achieving a statistically-representative, three-dimensional, microstructure characterization within a relatively large sample volume. While a tool for materials microstructure characterization in its own right, it is also suitable for providing input to finite-element modeling algorithms. It is based on a single, complex but manageable, approximation to the actual microstructure. The quality of the model for microstructure characterization should be assessed by comparison with other microstructure characterization methods. Its suitability for use as an input tool for FEM methods should be assessed by comparison of the resulting FEM-predicted properties with the measured properties for real samples.

Acknowledgements

The UNICAT facility at the Advanced Photon Source (APS) is supported by the U.S. DOE under Award No. DEFG02-91ER45439, through the Frederick Seitz Materials Research Laboratory at the University of Illinois at Urbana-Champaign, the Oak Ridge National Laboratory (U.S. DOE contract DE-AC05-00OR22725 with UT-Battelle LLC), the National Institute of Standards and Technology (U.S. Department of Commerce) and UOP LLC. The APS is supported by the U.S. DOE, Basic Energy Sciences, Office of Science under contract No. W-31-109-ENG-38.
This work was partially supported by the National Science Foundation MRSEC program at Stony Brook University under Grant No. DMR-0080021

Literature

1. He M.Y., J.W. Hutchinson, and A.G. Evans: Simulation of stresses and delamination in a plasma-sprayed thermal barrier system upon thermal cycling. Materials Science and Engineering A-Structural Materials Properties Microstructure and Processing 345 (2003), Issue 1-2, pp. 172-78.
2. Kokini K., A. Banerjee, and T.A. Taylor: Thermal fracture of interfaces in precracked thermal barrier coatings. Materials Science and Engineering A-Structural Materials Properties Microstructure and Processing 323 (200), Issue 1-2, pp. 70-82.
3. Nakamura T., and Z. Wang: Simulations of crack propagation in porous materials. Journal of Applied Mechanics-Transactions of the ASME 68 (2001), Issue 2, pp. 242-51.
4. Zimmermann A., W.C. Carter, and E.R. Fuller: Damage evolution during microcracking of brittle solids. Acta Materialia 49 (2001), Issue 1, pp. 127-37.
5. Ilavsky J., G.G. Long, A.J. Allen, L. Leblanc, M. Prystay, and C. Moreau: Anisotropic microstructure of plasma-sprayed deposits. Journal of Thermal Spray Technology 8 (1999), Issue 3, pp. 414-20.
6. Ilavsky J., G.G. Long, A.J. Allen, and C.C. Berndt: Evolution of the void structure in plasma-sprayed YSZ deposits during heating. Materials Science and Engineering a-Structural Materials Properties Microstructure and Processing 272 (1999), Issue 1, pp. 215-21.